

Numerical Method for the Stability Analysis of Ideal MHD Modes with a Wide Range of Toroidal Mode Numbers in Tokamaks

Nobuyuki AIBA, Shinji TOKUDA, Takaaki FUJITA, Takahisa OZEKI, Ming S. CHU¹⁾, Philip B. SNYDER¹⁾ and Howard R. WILSON²⁾

Japan Atomic Energy Agency, Naka 311-0193 Japan

¹⁾*General Atomics, PO Box 85608, San Diego, CA 92186-5608, USA*

²⁾*Department of Physics, University of York, Heslington, York YO10 5DD, UK*

(Received 30 November 2006 / Accepted 19 January 2007)

A numerical method for the stability analysis of ideal MHD modes is devised by using a physical model based on the two-dimensional Newcomb equation in combination with the conventional ideal MHD model. The MARG2D code based on this numerical method is able to analyze the stability of ideal MHD modes with a wide range of toroidal mode numbers. The validity of the MARG2D code has been confirmed through benchmarking tests using the DCON code for the low toroidal mode number MHD mode analysis, and tests using the ELITE code for intermediate to high toroidal mode number mode analysis. By using the MARG2D code, the MHD stability property of JT-60SA, the complementary device of ITER, is investigated with a focus on the effect of the plasma shape.

© 2007 The Japan Society of Plasma Science and Nuclear Fusion Research

Keywords: tokamak, ideal MHD stability, ELMs, Newcomb equation

DOI: 10.1585/pfr.2.010

1. Introduction

Magnetohydrodynamic (MHD) instability has become considered as one of key issues for the high performance operation in tokamaks. Low- n , n being the toroidal mode number, external (free boundary) MHD modes often limit plasma performance, and many authors have investigated the stability of these modes, for example in Refs. [1, 2]. In addition, intermediate to high- n external modes are considered to be one of the causes of edge localized modes (ELMs) which constrain the maximum pressure gradient in the pedestal at the tokamak edge region [3].

Numerical codes for estimating the linear growth rate γ of low- n ideal MHD modes in tokamaks have been developed. However, since there is the accumulating point of the continuous spectrum at the marginal stability point ($\gamma = 0$), it is difficult to identify the stability boundary explicitly using these codes. The PEST-II code was developed to identify the stability boundary by making the lower bound of the continuum a nonzero value in the stable region [4]. Recently, an innovative physical model to identify the stability boundary of ideal MHD modes in tokamaks has been devised [5]. With this model, the spectra of the eigenvalue problem are comprised of only the real and denumerable eigenvalues without continua. On the basis of this model, the MARG2D code has been developed. This code is able to identify the stability boundary of low- n ideal MHD modes by estimating the vacuum energy integral with the Green function method [6].

For the stability analysis of intermediate to high- n MHD modes of tokamak edge plasmas, some numerical codes have been developed recently [7–9]. These are applied to the numerical analysis of ELMy H-mode plasmas in existing devices and in ITER, and these analyses have revealed that type-I ELMs are induced by ideal MHD modes destabilizing near the plasma surface. To analyze the stability of tokamak edge plasmas using MARG2D, the physical model of MARG2D is extended to the vacuum region with the vector potential method [10].

As an analysis of edge MHD stability using MARG2D, we have reported the effect of the plasma shape at the top or the bottom of the equilibrium on the edge MHD stability [11]. In Ref. [11], we have shown that a ballooning mode and a peeling-ballooning mode are stabilized by sharpening the top or the bottom of the outermost magnetic surface, though a current-driven kink (peeling) mode is hardly stabilized. This stabilizing effect is caused by multiplying the local shear near the top or the bottom of the plasma, which stabilizes mainly the pressure-driven ballooning mode. These results have revealed that the plasma pressure at the pedestal can improve by sharpening the outermost surface.

The MARG2D code based on the physical model with the two-dimensional Newcomb equation can precisely identify the stability boundary of ideal MHD modes, but the eigenvalues computed by MARG2D correspond neither to γ nor to the frequencies of ideal MHD perturbations. To overcome this weakness, the plasma inertia

author's e-mail: aiba.nobuyuki@jaea.go.jp

considered in the conventional ideal MHD model under the incompressible assumption is implemented in MARG2D. By solving the eigenvalue problem with this plasma inertia after identifying whether the plasma is stable or unstable by using the model based on the Newcomb equation, a compressionless growth rate can be estimated. This numerical method has an advantage not only for numerical predictions of the plasma performance in existing and future experiments but also for integrated simulations realized by combining MARG2D with a tokamak transport code [12].

This paper is organized as follows. In Sec. 2, the development of the MARG2D code for estimating a compressionless growth rate is described. Section 3 describes the results of benchmarking tests of the MARG2D code by using the DCON code [13] by identifying the stability boundary of low- n MHD modes, and the results of tests by using the ELITE code [7, 8] by analyzing the intermediate to high- n MHD mode stability. In Sec. 4, the MHD stability property in JT-60SA [14], which is now under design as the complementary device of ITER, is investigated using MARG2D, focusing on an effect of the plasma shape. Section 5 presents a summary of this work.

2. Development of the Numerical Method of the MARG2D Code

In this section, we introduce the development of the numerical method used in the MARG2D code utilizing the compressionless ideal MHD model. We first define the straight field line flux coordinate system (r, θ, ϕ) as

$$r^2(\psi) = 2R_0 \int_0^\psi \frac{q}{F} d\psi, \quad (1)$$

$$\frac{\mathbf{B} \cdot \nabla \theta}{\mathbf{B} \cdot \nabla \phi} = q(\psi), \quad (2)$$

where ψ is the poloidal magnetic flux, F is the toroidal magnetic function, R_0 is the major radius, and q is the safety factor [15]. In this coordinate system, the Jacobian $\sqrt{g(r, \theta)}$ is given as

$$\sqrt{g(r, \theta)} = \frac{rR^2}{R_0}, \quad (3)$$

where R is the coordinate in the cylindrical coordinate system (R, Z, ϕ) . The MARG2D code solves numerically the eigenvalue problem associated with the two-dimensional Newcomb equation in this coordinate system [5]:

$$\mathcal{N}X(r) = -\lambda \mathcal{R}X(r). \quad (4)$$

Here \mathcal{N} is the Newcomb operator, λ is the eigenvalue, \mathcal{R} is a diagonal operator whose components are $\mathcal{R}_{m,m} \propto (m/q - n)^2$, m is the poloidal mode number, n is the toroidal mode

number, $X(r)$ is the vector function defined as

$$X(r) = \{X_{-L_f}(r), \dots, X_{L_f}(r)\}^t, \quad (5)$$

$$\xi \cdot \nabla r = X(r, \theta) = \sum_{l=-L_f}^{L_f} X_l(r) \exp(il\theta), \quad (6)$$

ξ is the plasma displacement with n ; L_f is the truncated poloidal mode number, and i is the complex unit. By introducing the solenoidal field C_V ($\nabla \cdot C_V = 0$) and the unknown vector ξ_V to express the perturbed magnetic field in the vacuum Q_V as

$$Q_V = \nabla \times A_V, \quad A_V = \xi_V \times C_V, \quad (7)$$

the Newcomb operator in Eq. (4) can be extended to the vacuum region, and a broad n range of external mode analyses can be realized using the MARG2D code [10].

By artificially choosing the weight function of the right hand side of Eq. (4) and imposing the natural boundary condition for the resonant harmonic at each rational surface, the spectra λ of Eq. (4) are comprised of real and denumerable eigenvalues without continuous spectra. This enables to identify explicitly the stability of the plasma with the sign of the minimum eigenvalue, but the eigenvalues correspond neither to γ nor to the frequencies of ideal MHD perturbations. However, if we already know that the plasma is unstable, the linear growth rates of ideal MHD modes can be estimated numerically based on the conventional ideal MHD model, because an ideal MHD spectrum contains continua in the stable side ($\gamma^2 \leq 0$) [16].

To realize both the identification of the stability boundary and the estimation of the linear growth rates using the single MHD spectrum code, we implement the physical plasma inertia under the assumption of incompressibility in MARG2D instead of the weight function in Eq. (4). The kinetic energy in the ideal MHD model can be written as

$$K = \frac{\gamma^2}{2} \int \rho |\xi|^2 \sqrt{g(r, \theta)} dr d\theta d\phi, \quad (8)$$

where ρ is the plasma density. We assume that the equilibrium is axisymmetric, the plasma density is constant as $\rho = \rho_0$, and the plasma is incompressible. With these assumptions, K can be given by

$$K = \pi \rho_0 \gamma_{\text{IM}}^2 \int \left(\frac{rR^2}{R_0 |\nabla r|^2} |X(r, \theta)|^2 + \frac{r |\nabla r|^2 R^4}{R_0^3} |V(r, \theta) - r \beta_{r,\theta} X(r, \theta)|^2 \right) dr d\theta, \quad (9)$$

$$V(r, \theta) = r \left(\xi \cdot \nabla \theta - \frac{1}{q} \xi \cdot \nabla \phi \right), \quad (10)$$

where γ_{IM} is the compressionless growth rate, and $\beta_{r,\theta}$ is the measure of nonorthogonality of the (r, θ, ϕ) coordinate system defined as

$$\beta_{r,\theta}(r, \theta) = \frac{\nabla r \cdot \nabla \theta}{|\nabla r|^2}. \quad (11)$$

Since the variable $V(r, \theta)$ can be solved analytically as a function of $X(r)$ in the MARG2D formulation [5], K in Eq. (9) can be expressed in the quadratic form of $X(r)$ as

$$K = 2\pi^2 \rho_0 \gamma_{\text{IM}}^2 \int_0^a \langle X | \mathcal{K} | X \rangle dr, \quad (12)$$

where a is the plasma minor radius, and the bracket of vectors \mathbf{a} and \mathbf{c} and a matrix \mathcal{B} , $\langle \mathbf{a} | \mathcal{B} | \mathbf{c} \rangle$, is defined as

$$\langle \mathbf{a} | \mathcal{B} | \mathbf{c} \rangle = \mathbf{a}^t \mathcal{B} \mathbf{c} = \sum_{j,k} a_j \mathcal{B}_{j,k} c_k. \quad (13)$$

Since the plasma potential energy W_p has also been expressed in the quadratic form of $X(r)$ [5], the stationary condition of the functional

$$\mathcal{W}[X] = W_p + \gamma_{\text{IM}}^2 K \quad (14)$$

for arbitrary variations of $X(r)$ yields an eigenvalue problem:

$$\mathcal{N}X(r) = \gamma_{\text{IM}}^2 \mathcal{K}X(r). \quad (15)$$

MARG2D can estimate the compressionless growth rate γ_{IM} by solving this eigenvalue problem with the continuous condition for each $X_i(r)$ at rational surfaces after identifying whether the plasma is stable or unstable by solving Eq. (4).

3. Benchmarking Test of MARG2D

In this section, the results of benchmarking tests of the MARG2D code are shown. Benchmarking tests of the low- n mode analysis in an up-down symmetric equilibrium have previously been executed in Refs. [10, 17]. Hence, in Subsec. 3.1, we first compare the stability boundaries of $n = 1, 2, 3$ external MHD modes identified by using the MARG2D and the DCON codes [13] in an up-down asymmetric equilibrium. Next, in Subsec. 3.2, the stability of $5 \leq n \leq 100$ ideal MHD modes in an up-down symmetric equilibrium is analyzed using the MARG2D and the ELITE codes as the benchmarking test of intermediate to high- n mode analysis.

3.1 Benchmarking for identifying the stability boundary of low- n MHD modes

As the benchmarking test for identifying the stability boundary of low- n MHD modes, we use MARG2D and DCON to investigate the dependence of the β_N limit on the position of the conducting wall surrounding the plasma d/a , where β_N is the normalized beta value defined as $\beta_N \equiv 100 \beta_t a B_t / I_p$, β_t [%] is the toroidal beta, B_t [T] is the toroidal magnetic field on the axis, I_p [MA] is the plasma current, d is the radius of the wall defined as

$$2d = R_w(Z=0)|_{\text{out}} - R_w(Z=0)|_{\text{in}}, \quad (16)$$

R_w is the R coordinate of the wall on the (R, Z) plane, and subscript in (out) indicates the position inside (outside) of

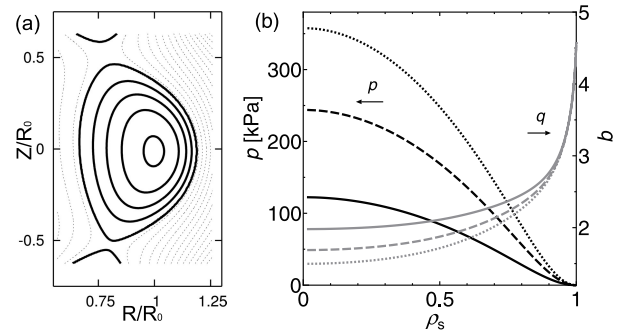


Fig. 1 (a) Contour of the poloidal magnetic flux $\psi = \text{const.}$ of $\beta_N = 5.5$ equilibrium. (b) Profiles of pressure p (black) and safety factor q (gray) when $\beta_N = 3.0$ (solid line), 5.5 (broken line), and 7.5 (dotted line), respectively.

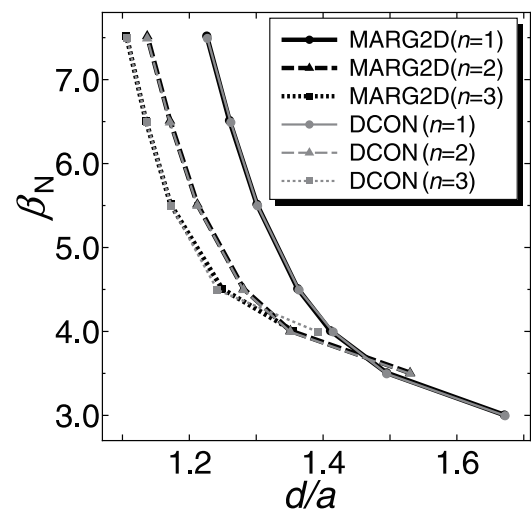


Fig. 2 Dependence of the β_N limit on the wall position d/a . Each dependence of the β_N limit restricted by the $n = 1, 2, 3$ MHD modes stability estimated with MARG2D is almost identical to that calculated with DCON.

the magnetic axis. The distance from the plasma surface to the wall is fixed as $d - a$. A series of equilibria is obtained by solving the Grad-Shafranov equation numerically using the MEUDAS equilibrium code [18]. When the β_N value of the equilibrium is changed from 3.0 to 7.5, the shape of the outermost closed surface and the safety factor at the plasma edge q_{edge} are fixed as R_0 [m] = 3.24, a [m] = 0.84, and $q_{\text{edge}} = 4.58$. The contours of $\psi = \text{const.}$ (magnetic surfaces) when $\beta_N = 5.5$, and the profiles of plasma pressure p and q when $\beta_N = 3.0, 5.5$, and 7.5 are shown in Fig. 1. The transverse value in Fig. 1 (b) is defined as $\rho_s = \sqrt{\psi_N}$, where ψ_N is a normalized poloidal flux as $\psi_N = 0$ at the axis and $\psi_N = 1$ at the surface. MARG2D and DCON identify the stability boundaries of $n = 1, 2, 3$ MHD modes in this series of equilibria.

Figure 2 shows the dependence of the β_N limit on d/a . These dependences revealed by MARG2D and DCON are almost identical to each other. Unfortunately, since

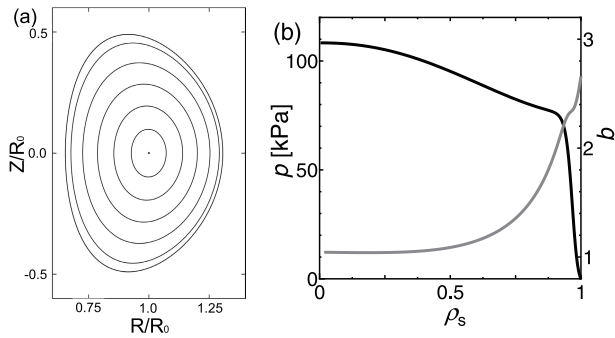


Fig. 3 (a) Contour of the poloidal magnetic flux $\psi = \text{const.}$ (b) Profiles of pressure p (black) and safety factor q (gray), respectively.

the DCON code used in this benchmarking (ver. 3.2) cannot output an eigenfunction, we cannot compare the radial structure of the eigenfunction with that determined by MARG2D. However, in an up-down symmetric equilibrium, the benchmarking tests between the MARG2D and the ERATOJ codes [19] have been executed in Refs. [10, 17], and the radial structures of the marginally stable eigenfunctions have been identified as almost identical. These results demonstrate that the stability boundary of low- n MHD modes identified by means of MARG2D is accurate.

3.2 Benchmarking for the stability analysis of intermediate to high- n MHD modes

As the benchmarking test of intermediate to high- n mode stability analysis, the compressionless growth rates γ_{IM} of $5 \leq n \leq 100$ ideal MHD modes are calculated using the MARG2D and the ELITE codes [7, 8]. The equilibrium used in this benchmarking is calculated using the TOQ code [20]. Figure 3 shows the contour of $\psi = \text{const.}$, and the profiles of p and q . The equilibrium quantities are $R_0[\text{m}] = 3.00$, $a[\text{m}] = 0.97$, $\beta_N = 2.83$, $I_p[\text{MA}] = 2.70$, and $B_t[\text{T}] = 3.00$.

The results of the stability analysis of $5 \leq n \leq 100$ MHD modes are shown in Fig. 4. Figure 4(a) shows the n dependence of γ_{IM} normalized with the toroidal Alfvén frequency on the magnetic axis ω_A . The agreement between the results of MARG2D and ELITE is quite close, and the radial structures of the most unstable eigenfunction obtained using MARG2D (Fig. 4(b)) and ELITE (Fig. 4(c)), whose n number is 10, are almost identical to each other. These structures consist of a combination of a peeling component peaking at the plasma surface and a ballooning component whose envelope maximum is near $\rho_s = 0.92$.

These results shown in this section confirm that the MARG2D code can determine the stability of the wide n range of ideal MHD modes with a high level of accuracy.

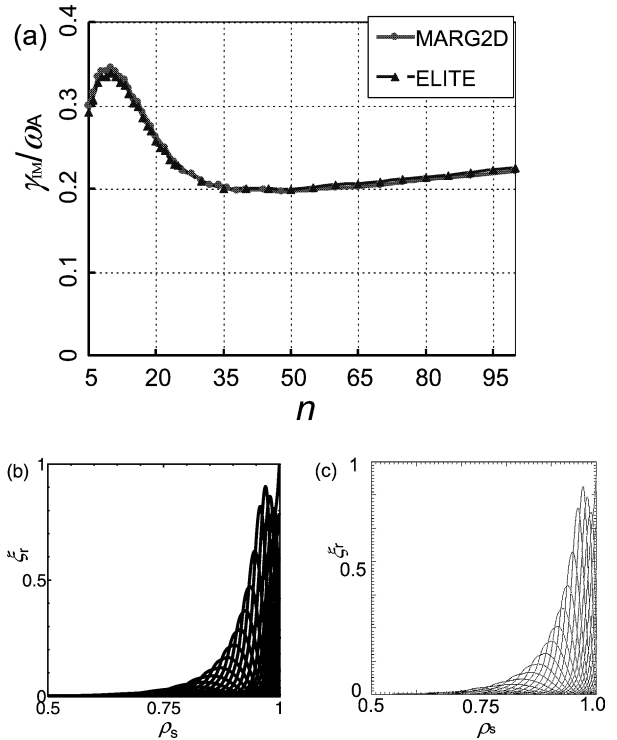


Fig. 4 (a) Dependence of $\gamma_{\text{IM}}/\omega_A$ on n calculated with MARG2D (solid line) and ELITE (broken line). The agreement between both codes is quite close. Radial structures of the most unstable eigenfunction whose $n = 10$ calculated with (b) MARG2D and (c) ELITE are also almost identical to each other.

4. Stability Analysis in JT-60SA Plasmas Using MARG2D

In this section, we show the results of ideal MHD stability analysis in JT-60SA plasmas. Since JT-60SA is designed to have a flexible plasma shape, we focus on effects of the plasma shape on MHD stability. The effect of the plasma shape on the β_N limit determined by low- n MHD stability is investigated in Subsec. 4.1, and the shaping effect on the edge MHD stability is analyzed in Subsec. 4.2.

4.1 Low- n MHD mode analysis in JT-60SA plasmas

As the complementary device of ITER, JT-60SA is now under design by the JA-EU satellite tokamak working group and the JT-60SA design team [14]. To support and supplement ITER toward a future demonstration reactor DEMO, JT-60SA will have a flexibility of the plasma shape. In this subsection, we analyze the stability of ideal MHD modes in the variously shaped JT-60SA plasmas, and investigate the effect of the plasma shape on the β_N limit determined by the stability of low- n MHD modes.

Figure 5 shows the contours of $\psi = \text{const.}$ (magnetic surfaces) of (a) an ‘ITER-like’ shape equilibrium (later written as ITER-like Eq.) and (b) a so-called

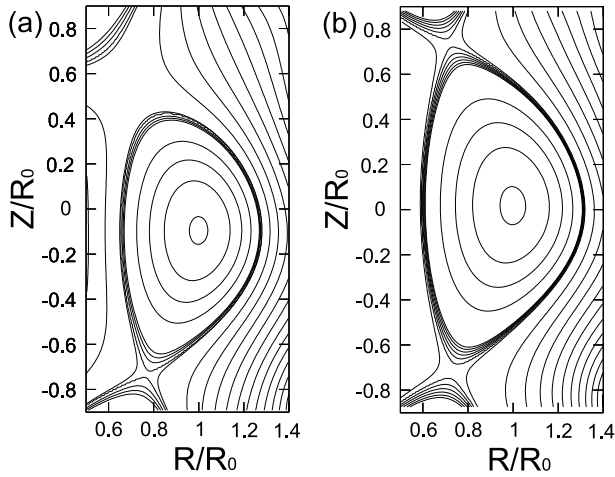


Fig. 5 Contours of $\psi = \text{const.}$ (magnetic surfaces) of (a) the ITER-like Eq. and (b) the high- S Eq.

‘high- S ’ shape equilibrium (high- S Eq.) in JT-60SA, where S is the shaping factor defined as $S = q_{95}I_p/aB_t$, and q_{95} is the safety factor q at 95% of the flux surface. The shaping parameters ($R_0, a, \kappa_{\text{up}}, \kappa_{\text{dw}}, \delta_{\text{up}}, \delta_{\text{dw}}$) are (3.00, 0.97, 1.66, 2.01, 0.34, 0.60) in the ITER-like Eq. and (3.03, 1.15, 1.96, 1.96, 0.63, 0.56) in the high- S Eq., where κ is the ellipticity, δ is the triangularity, and the subscript up (dw) indicates the up (down) side value. The B_t and I_p values are $(B_t, I_p) = (2.49, 2.59)$ in the ITER-like Eq. and $(2.60, 5.00)$ in the high- S Eq. Profiles of pressure gradient and averaged parallel current density are given as

$$\frac{dp}{d\psi} \propto (1 - \psi_N^{3,0})^{1.2} + C_p \left(\exp\left(-\frac{(\psi_N - 0.94)^2}{2 \times (0.03)^2}\right) \right), \quad (17)$$

$$\langle \mathbf{j} \cdot \mathbf{B} \rangle \propto (1 - \psi_N^{C_2})^{C_3} + C_j \left(\exp\left(-\frac{(\psi_N - 0.94)^2}{2 \times (0.03)^2}\right) \right). \quad (18)$$

Here \mathbf{j} is the plasma current density, and the bracket $\langle X \rangle$ expresses the flux surface average of a variable X . The pressure gradient and the current density near $\psi_N = 0.94$ are changed by adjusting the parameters C_p and C_j , which are used to express the edge pedestal and the virtual bootstrap current, and the parameters C_{j2}, C_{j3} are adjusted for changing the global current profile.

Figure 6 shows the profiles of (a) p and (b) q of the ITER-like Eq. (black) and the high- S Eq. (gray) when β_N is fixed as 4.0. The solid lines express the L-mode profiles whose parameters (C_p, C_j) in Eqs. (17) and (18) are (0.2, 0.18) in the ITER-like Eq. and (0.2, 0.2) in the high- S Eq., and the broken lines indicate the H-mode profiles whose (C_p, C_j) are (0.6, 0.25) and (0.6, 0.3) in the ITER-like and the high- S equilibria, respectively. For β_N limit analysis, a series of different β_N equilibria has the similar q profile whose q value at the magnetic axis is $q_0 = 1.20$ and $q_{\text{edge}} = 5.63$ by adjusting I_p and the parameters C_{j2}

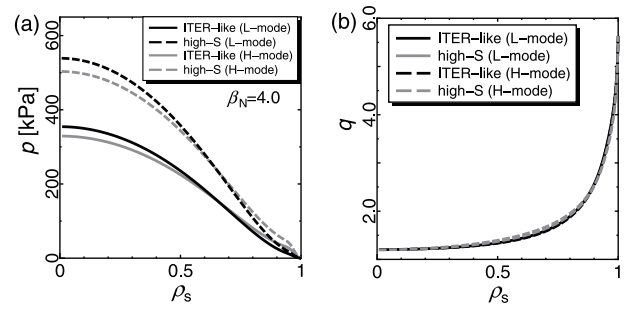


Fig. 6 Profiles of (a) pressure p and that of (b) safety factor q in the ITER-like Eq. (black) and the high- S Eq. (gray) when $\beta_N = 4.0$. The solid and broken lines show the L-mode profiles and the H-mode profiles, respectively. The q profiles of these equilibria are almost identical to each other.

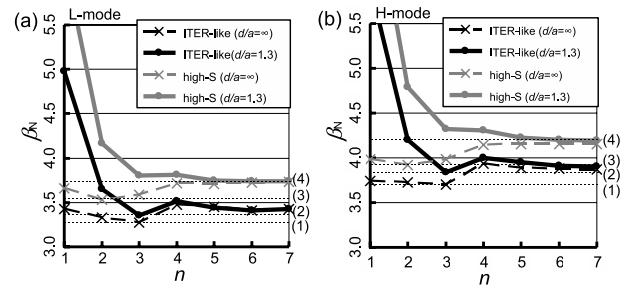


Fig. 7 Dependence of the β_N limit on the toroidal mode number n of the MHD modes in the ITER-like Eq. (black) and the high- S Eq. (gray) ((a) L-mode profile case, (b) H-mode profile case). The solid lines show the β_N limit when $d/a = 1.3$ and the broken lines express that when $d/a = \infty$. The β_N limits when the equilibria have the L-mode profile, shown in (a), are (1) 3.27 ($d/a = \infty$) and (2) 3.36 (1.3) in the ITER-like Eq., and those are (3) 3.53 ($d/a = \infty$) and (4) 3.75 (1.3) in the high- S Eq., respectively. In the H-mode profile case shown in (b), the β_N limits are (1) 3.71 ($d/a = \infty$) and (2) 3.75 (1.3) in the ITER-like Eq., and those are (3) 4.15 ($d/a = \infty$) and (4) 4.23 (1.3) in the high- S Eq.

and C_{j3} in Eq. (18). For example, when $\beta_N = 4.0$ as shown in Fig. 6, (I_p, C_{j2}, C_{j3}) are adjusted as (2.84, 2.55, 1.5) and (2.81, 2.42, 1.5) in the ITER-like L-mode and H-mode equilibria, and (5.03, 3.34, 1.0) and (5.06, 2.85, 1.0) in the high- S L-mode and H-mode equilibria.

Figure 7 shows the β_N limit determined by the stability of $1 \leq n \leq 7$ MHD modes in (a) the L-mode and (b) the H-mode equilibria where the black lines show the results of the ITER-like Eq., and the gray lines show those of the high- S Eq. The solid lines show the results when the conducting wall surrounding the plasma is placed at $d/a = 1.3$ and the broken lines indicate the no wall condition ($d/a = \infty$) results. In the ITER-like L-mode profile case, the β_N limit determined by the $n = 3$ MHD mode stability is 3.27 when $d/a = \infty$ (shown with dotted line (1) in Fig. 7 (a)), and this value changes little when the conduct-

ing wall is placed close to the plasma surface $d/a = 1.3$ (dotted line (2)). The β_N limit of the high- S L-mode Eq., determined by the $n = 2$ MHD mode stability, is 3.53 when $d/a = \infty$, which is larger than that of the ITER-like L-mode Eq. Since lower- n MHD modes can be stabilized effectively by bringing the conducting wall close to the plasma surface, the β_N limit increases from 3.53 to 3.75 and the n number of the MHD mode determining the β_N limit changes from 2 to 5 by changing d/a from ∞ to 1.3 in this high- S L-mode Eq. case. In the H-mode profile case shown in Fig. 7 (b), the β_N limit becomes larger than that in the L-mode profile case, because the edge pedestal raises the level of the plasma pressure near the surface and reduces that of the plasma core region as shown in Fig. 6 (a). The high- S Eq. also has a larger β_N limit than that of the ITER-like Eq. as in the L-mode case. When $d/a = 1.3$, for example, the β_N limit of the high- S Eq. reaches about 4.23, which is larger than that of the ITER-like Eq. (= 3.75).

From these results, we confirm that the high- S equilibrium is suitable for a high performance discharge whose $\beta_N \geq 3.5$, and MARG2D is a powerful tool to investigate an optimized equilibrium profile by analyzing the β_N limit in the various equilibria.

4.2 Stability analysis in JT-60SA edge plasma

As is well known, the MHD stability of tokamak edge plasmas is responsible for ELM phenomena. Moreover, since a plasma performance depends on the edge pressure gradient as shown in the previous subsection, the edge MHD stability is also important for achieving high performance discharges. In this subsection, the stability of edge-localized MHD modes in JT-60SA plasma is analyzed using MARG2D.

The equilibria to be analyzed are the ITER-like Eq. and the high- S Eq. whose magnetic surface shapes are shown in Fig. 5. In this analysis, the B_t and I_p values are

fixed as $(B_t, I_p) = (2.49, 2.59)$ in the ITER-like Eq. and $(2.60, 5.00)$ in the high- S Eq., and the profiles of pressure gradient and averaged parallel current density are given as Eqs. (17) and (18). The parameters (C_{j2}, C_{j3}) are fixed as $(2.4, 1.0)$ in each equilibrium, and the pressure gradient and the current density near $\psi_N = 0.94$ are changed by adjusting the parameters C_p and C_j . The poloidal beta value β_p is fixed as 0.8, and the q_{edge} values of these equilibria are similar to each other when the parameter C_j is fixed. Figure 8 shows the profiles of (a) pressure p (solid line) and pressure gradient $dp/d\psi$ (broken line), and that of (b) safety factor q (solid line) and $\langle j \cdot B \rangle$ when $C_p = 2.0$ and $C_j = 0.3$. The black and the gray lines show the profiles of the ITER-like Eq. and those of the high- S Eq. The position of the wall is fixed as $d/a = 1.3$, and the stability of the MHD mode whose n varies from 1 to 60 is analyzed using MARG2D, and the stability boundary of the infinite- n ballooning mode is analyzed using the BETA code [21].

Figure 9 (a) shows the result of the stability analysis of the MHD modes on the $j_{//\text{edge}}/\langle j_{//} \rangle - \alpha_{94}$ diagram

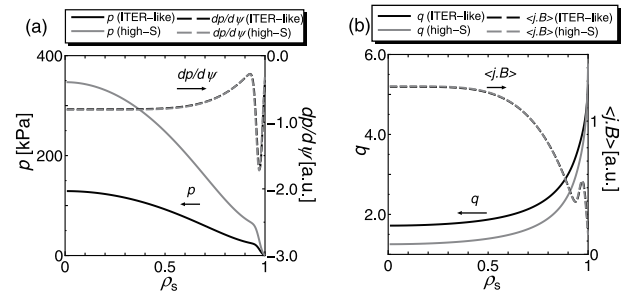


Fig. 8 Profiles of (a) pressure p (solid line) and pressure gradient $dp/d\psi$ (broken line), and those of (b) safety factor q (solid line) and $\langle j \cdot B \rangle$ (broken line) when $C_p = 2.0$ and $C_j = 0.3$. The black and the gray lines show the ITER-like Eq. profiles and the high- S Eq. profiles, respectively.

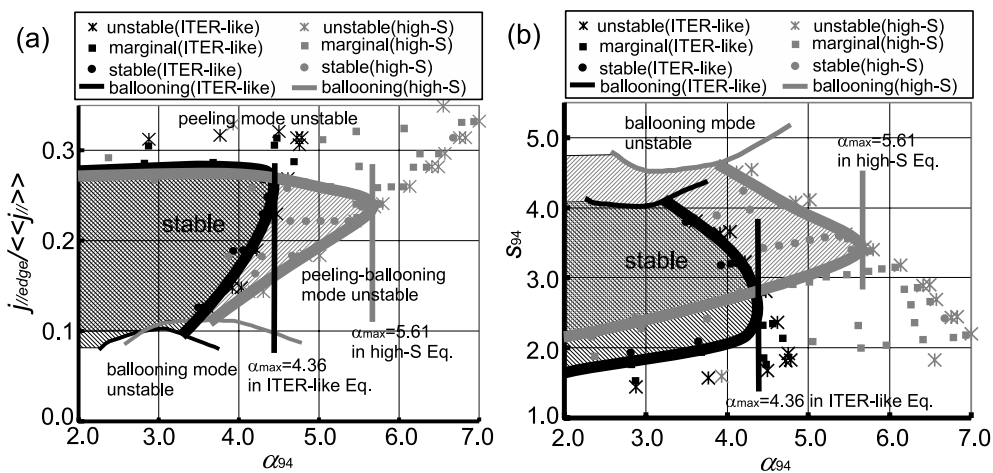


Fig. 9 Stability diagrams of the ITER-like Eq. (black) and the high- S Eq. (gray) on (a) the $(j_{//\text{edge}}/\langle j_{//} \rangle, \alpha_{94})$ plane and (b) the (s_{94}, α_{94}) plane. The maximum α_{94} value is 4.36 in the ITER-like Eq. and 5.61 in the high- S Eq.

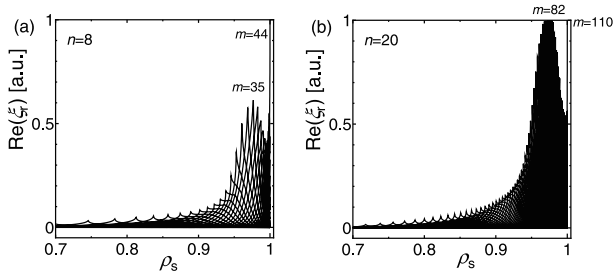


Fig. 10 Radial structures of the eigenfunction restricting the maximum α_{94} value in (a) the ITER-like Eq. ($\alpha_{94} = 4.36$) and (b) the high- S Eq. ($\alpha_{94} = 5.61$). The toroidal mode number n of the eigenfunction is 8 in the ITER-like Eq. and 20 in the high- S Eq., respectively.

of the ITER-like Eq. (black) and the high- S Eq. (gray), where $j_{||}$ is the current density parallel to the magnetic field, $j_{||\text{edge}}$ is the flux surface averaged $j_{||}$ at the plasma edge, the bracket $\langle\langle X \rangle\rangle$ expresses the cross-section area average of a variable X , α is the normalized pressure gradient defined as $\alpha = -2\mu_0 R q^2 (dp/dr)/B^2$, μ_0 is the permeability in the vacuum, r is the minor radius of each magnetic surface, and the subscript 94 indicates the value at $\psi_N = 0.94$. In this figure, reference symbols, cubic symbols, and circle symbols indicate the unstable points ($\gamma_{\text{IM}}/\omega_A \geq 5.00 \times 10^{-3}$), the marginal points ($0.00 < \gamma_{\text{IM}}/\omega_A < 5.00 \times 10^{-3}$), and the stable points ($\gamma_{\text{IM}}/\omega_A \leq 0.00$), respectively. This result shows that the maximum α_{94} value in the high- S Eq. ($\alpha_{94\text{max}} = 5.61$) becomes larger than that in the ITER-like Eq. ($\alpha_{94\text{max}} = 4.36$) by changing to the strongly shaped plasma. Since the q_{edge} value remains fixed when the $(j_{||\text{edge}}/\langle\langle j_{||} \rangle\rangle)$ value is unchanged, the maximum $(j_{||\text{edge}}/\langle\langle j_{||} \rangle\rangle)$ value against peeling (kink) modes is almost the same about 0.28 in each equilibrium. In other words, the stability of the current-driven modes hardly depends on the shaping factor S . On the other hand, from the $s_{94} - \alpha_{94}$ diagram shown in Fig. 9 (b), we find that the second stable region against the infinite- n ideal ballooning mode in the high- S Eq. is broader than that in the ITER-like Eq., where s is the magnetic shear defined as $s = r(dq/dr)/q$. These results, shown in Figs. 9 (a) and (b), indicate that the pressure-driven component is stabilized by increasing the shaping factor S . This stabilization enhances the maximum pressure gradient determined by the peeling-ballooning mode stability.

The radial structure of the eigenfunction restricting the maximum α_{94} value is shown in Fig. 10. In the ITER-like Eq. case shown in Fig. 10 (a), the n number of the mode is 8, and the peeling component peaking at the plasma surface is dominant. As shown in Fig. 10 (b), the dominant component of the eigenfunction in the high- S Eq. case, whose n number is 20, is the ballooning component whose envelope maximum is near $\rho_s = 0.97$. Though this result in the high- S Eq. case is different from the result in the ITER-like Eq. case, the width of the radial structure

is similar to that in the ITER-like Eq. case. From the viewpoint of a width of the eigenfunction, the crash width of the pedestal induced by destabilizing these peeling-ballooning modes changes little in either equilibria.

From these results, we study that the edge MHD stability can be improved by varying the plasma shape from the ITER-like shape to the high- S shape in JT-60SA plasmas without changing the width of the eigenfunction of the MHD mode restricting the maximum pressure gradient.

5. Summary

We have devised an effective numerical method for the stability analysis of ideal MHD modes using a physical model based on the two-dimensional Newcomb equation in combination with the conventional compressionless ideal MHD model. The MARG2D code has been developed based on this numerical method, and this code is able to analyze the stability of ideal MHD modes with a wide range of toroidal mode numbers. The validity of the MARG2D code has been confirmed through the benchmarking tests using the DCON code for low toroidal mode number MHD mode analysis, and those using the ELITE code for intermediate to high toroidal mode number mode analysis. By means of the MARG2D code, we have investigated the MHD stability property in JT-60SA, the complementary device of ITER, focusing on an effect of the plasma shape. These stability analyses show that the highly shaped plasma designed for achieving high performance discharges in JT-60SA is suitable for stabilizing not only low toroidal mode number MHD modes, which restrict the β_N discharge limits, but also intermediate to high toroidal mode number MHD modes, which relate to edge pedestal performance and ELM phenomena. As demonstrated by the numerical analyses described in this paper, MARG2D can effectively perform stability analyses of the various kinds of ideal MHD modes needed for the experimental analysis of existing devices and the design of ITER and JT-60SA.

The numerical model shown in this paper can estimate the compressionless linear growth rate. The numerical model for calculating the growth rate with compression is desirable for experimental analyses and tokamak integrated simulations, and will be reported in the near future.

Acknowledgments

The authors would like to thank Dr. M. Kikuchi and Dr. H. Ninomiya for their support.

- [1] T. Ozeki *et al.*, Nucl. Fusion **35**, 861 (1995).
- [2] M.S. Chu, M.S. Chance, A.H. Glasser and M. Okabayashi, Nucl. Fusion **43**, 441 (2003).
- [3] J.W. Connor, R.J. Hastie, H.R. Wilson and R.L. Miller, Phys. Plasmas **5**, 2687 (1998).
- [4] R.C. Grimm, R.L. Dewar and J. Manickam, J. Comput. Phys. **49**, 94 (1983).

- [5] S. Tokuda and T. Watanabe, *Phys. Plasmas* **6**, 3012 (1999).
- [6] N. Aiba, S. Tokuda and T. Ishizawa, *J. Plasma Phys.* **72**, 1127 (2006).
- [7] H.R. Wilson, P.B. Snyder, R.L. Miller and G.T.A. Huysmans, *Phys. Plasmas* **9**, 1277 (2002).
- [8] P.B. Snyder *et al.*, *Phys. Plasmas* **9**, 2037 (2002).
- [9] A.B. Mikhailovskii, G.T.A. Huysmans, W.O.K. Kerner and S.E. Sharapov, *Plasma Phys. Rep.* **23**, 844 (1997).
- [10] N. Aiba, S. Tokuda, T. Ishizawa and M. Okamoto, *Comput. Phys. Commun.* **175**, 269 (2006).
- [11] N. Aiba, S. Tokuda, T. Takizuka, G. Kurita and T. Ozeki, *Nucl. Fusion* **47**, 297 (2007).
- [12] N. Hayashi, T. Takizuka, T. Ozeki, N. Aiba and N. Oyama, in *Proc. 21st IAEA Fusion Energy Conf.*, (Chengdu, 2006) (Vienna, IAEA) CDROM file TH/4-1 and <http://www-naweb.iaea.org/naweb/physics/FEC/FEC2006/html/index.html>.
- [13] A.H. Glasser and M.S. Chance, *Bull. Am. Phys. Soc.*, **42**, 1848 (1997).
- [14] M. Kikuchi, JA-EU satellite tokamak working group, and JT-60SA design team, in *Proc. 21st IAEA Fusion Energy Conf.*, (Chengdu, 2006) (Vienna, IAEA) CDROM file FT/2-5 and <http://www-naweb.iaea.org/naweb/physics/FEC/FEC2006/html/index.html>.
- [15] M.N. Bussac, R. Pellat, D. Edery and J.L. Soule, *Phys. Rev. Lett.* **35**, 1638 (1975).
- [16] J.P. Freidberg, *Ideal Magnetohydrodynamics* (Plenum Press, New York, 1987).
- [17] N. Aiba, S. Tokuda, T. Ishizawa and M. Okamoto, *Plasma Phys. Control. Fusion* **46**, 1699 (2004).
- [18] M. Azumi *et al.*, in *Proc. 4th Int. Symp. on Comput. Methods Applied Sci. Engineering, Paris* (North-Holland, Amsterdam, 1980) p.335.
- [19] R. Gruber and J. Rappaz, *Finite Elements Methods in Linear Ideal Magnetohydrodynamics* (Berlin: Springer, 1985).
- [20] R.L. Miller and J.W. Van Dam, *Nucl. Fusion* **27**, 2101 (1987).
- [21] M. Azumi *et al.*, in *Proc. 6th Int. Conf. Plasma Phys., Lausanne* (CEC, Brussels, 1984) Vol.1, p.200.